A newly identified spliceosomal protein Ahed is essential for homeostasis of the epidermis

Shigetoshi Sano (sano.derma@kochi-u.ac.jp)
Kōchi University https://orcid.org/0000-0002-9812-0216
Mikiro Takaishi
Kochi University
Tatsushi Ishimoto
Kochi University
Ken-ichi Yagyu
Kochi University
Sayo Kataoka
Kochi University
Motoki Kondo
Kochi University
Keiko Morisawa
Kochi Medical School Hospital
Sonoko Kinjo
National Institute of Genetics
Kazuho Ikeo
National Institute of Genetics
Shohei Noma
RIKEN Preventive Medicine and Diagnosis Innovation Program, Wako, Saitama, Japan
Chitose Takahashi
RIKEN Center for Integrative Medical Science
Yasushi Okazaki
RIKEN, Center for Integrative Medical Sciences
Masahiro Tokunaga
Suita Municipal Hospital
Chikara Kokubu
Department of Genome Biology, Graduate School of Medicine, Osaka University, Osaka, Japan
Junji Takeda
Research Institute for Microbial Diseases, Osaka University

Article

Keywords:

Posted Date: August 11th, 2023

DOI: https://doi.org/10.21203/rs.3.rs-3234334/v1

Additional Declarations: There is **NO** Competing Interest.

Abstract

To identify genes that are essential for cellular and organ functions, we established a homozygous mutant mouse embryonic stem cell bank from which we identified a gene, named *Attenuated Hematopoietic Development (Ahed)*, that plays an essential role in hematopoiesis. Here we characterize the role of *Ahed* in skin development by analyzing mice with an epidermis-specific Ahed deficiency (EcKO). Those mice have increased numbers of apoptotic cells in the epidermis from the fetal stage. Thereafter, Ahed-EcKO mice develop skin barrier disruptions over time, which cause lethality soon after birth, showing epidermal abnormalities including the loss of filaggrin and an increase of pro-inflammatory gene expression. Experiments using Tam/ERT2-mediated inducible *Ahed* deletion *in vivo* and *in vitro* revealed that an *Ahed* deficiency leads to keratinocyte apoptosis, impairs keratinocyte proliferation and promotes dermatitis development. Since we found that *Ahed* has a critical role in hematopoiesis as a spliceosomal protein that controls gene splicing of hematopoiesis-related molecules, we further characterized the protein interactions of Ahed with other spliceosomal proteins in HeLa cells, and identified the altered splicing of mRNAs in *Ahed*-deficient keratinocytes. These results suggest that *Ahed* plays an indispensable role in processing mRNAs during development and in maintaining skin integrity, and more importantly, it contributes to mRNA splicing that is essential for multiple cell lineages.

Introduction

In multicellular organisms, cells from each fertilized egg undergo repeated divisions, during which they acquire specific functions to generate tissues and organs. This process is brought about by the interactions of various molecules in a strictly controlled spatiotemporal manner. Recent advances in molecular genetics have revealed the underlying mechanisms of ontogeny, however, many aspects still remain elusive. Forward genetics has been an approach used to identify genes responsible for characteristic phenotypes and functions of a variety of organisms, such as C. elegans[1–3], D. melanogaster[4,5], zebrafish[6,7] and mice[8]. To obtain *in vivo* phenotypes of interest in rodents, random mutations were created by treatment with chemical mutagens, such as N-ethyl-N-nitrosourea (ENU)[9]. Gene-trap mutagenesis was performed with the introduction of various types of DNA fragments[8]. More recently, an RNA interference (RNAi) strategy was adopted for the *in vivo* screening of mice[10].

Horie et al. developed a novel method to produce and enrich homozygous mutant murine embryonic stem (ES) cell clones by transient suppression of the *Bloom syndrome* (*Blm*) gene[11]. Consequently, approximately 200 ES cell clones harboring specific gene mutations in both alleles were established. The roles for the target genes can be investigated by modification of the ES cell environment to induce a specific cell lineage from ES cell clones *in vitro*. By taking advantage of this strategy, we recently identified a novel gene in which a mutation resulted in abnormal hematopoietic differentiation *in vitro* in co-cultures with OP9 stromal cells, and therefore, that gene was named “attenuated hematopoietic development (*Ahed*)”[12]. Conventional *Ahed* deficient mice die *in utero* around E6.5, which is earlier than the beginning of hematopoiesis, which strongly suggests that *Ahed* is indispensable during early

ontogeny. Furthermore, a homozygous *Ahed* disruption in a hematopoietic cell-specific manner (Vav1Cre_Ahed flox/flox) led to severe anemia resulting in embryonic lethality around E14.5. Analyses of liver hematopoiesis and bone marrow from Vav1 promoter-mediated Ahed KO mice revealed that Ahed is indispensable for the production of functional hematopoietic stem/progenitor cells.

Self-renewing stem/progenitor cells can be mobilized into action when their tissue is injured in order to maintain homeostasis. Their cellular states during homeostasis are tightly regulated by cell-intrinsic and by cell–extrinsic mechanisms that encompass the bi-directional crosstalk between stem cells and their functional niche cells[13,14]. Given that stem/progenitor cells of the hematopoietic system are shared with those of the epidermis in renewal of their differentiation to progeny throughout life, we aimed to determine the role of *Ahed* in skin architecture during both ontogeny and adulthood.

The genesis of the epidermis in mice begins at embryonic day 9 (E9) when keratin (K) 8/18 is replaced by K 5/14, which represent the epidermal commitment[15]. Around E14, pilosebaceous units develop from epidermal downgrowths that give rise to epidermal thickenings, named placodes, through specific epithelial-mesenchymal interactions, which supply permissive and instructive signaling for the position of hairs and other appendages[16]. Hair follicles (HFs) protrude downwards from the epidermis into the dermis. The activation of HF stem cells determines the synchronized phases of rest (telogen), growth (anagen) and regression, known as the hair cycle. HF stem cells reside in the bulge and are quiescent in telogen but are active in anagen[13]. Spatiotemporal interactions between epithelial and mesenchymal cells, including niche cells, determine HF growth and postnatal homeostasis. The interfollicular epidermis (IFE) or stratified skin, which develops between HFs, is continuous with the outer root sheath of HFs. Asymmetric cell divisions in the basal layer of the IFE, where epidermal stem/progenitor cells are located, increase the number of cell layers and promote Notch-dependent epidermal differentiation[16]. Thus, a variety of cross-talks between intrinsic and extrinsic signals, including transcription factors and growth factors, contribute to the renewal and homeostasis of HFs and the epidermis.

Since we expected a potential correlation of *Ahed* (as a previously uncharacterized gene *AU019823*) with the RNA splicing process from the BioPlex 3.0 database, transcriptome analysis revealed that hematopoietic stem/progenitor cells from an *Ahed*-deficient mouse fetus express alternatively spliced transcripts, including hematopoiesis-related genes[12]. However, details of the molecular mechanism(s) underlying the function of Ahed remained unknown. In the present study, we explored the role of Ahed in skin development and further delineate the inter-molecule interactions of Ahed and other spliceosomal complex proteins.

Results

Embryonic skin of epidermis-specific Ahed knockout (KO) mice

First, we investigated skin development in mice with an Ahed deficiency. To this end, epidermis-specific Ahed deficient (Ahed-EcKO) mice were generated by crossing Ahed $^{flox/flox}$ mice[12] with K5.Cre mice. Ahed-EcKO mice were born according to Mendelian's law. Histological examination of embryos of Ahed-EcKO mice on 19.5 days post-coitum (dpc 19.5), revealed increased numbers of apoptotic cells in the epidermis, showing eosinophilic and pyknotic cells with H&E staining and TUNEL positivity compared with wild-type mice (Fig. 1a, b). Although Ahed-EcKO embryos had no obvious alterations in their epidermal structure by H&E staining, filaggrin (FLG) expression was decreased in Ahed-EcKO skin compared with control mice (Fig. 1a). qRT-PCR analysis of embryonic skin revealed slight but significant decreases in mRNA levels of *Flg*, *Casp14* and HF development genes and stem cell signature genes, including *p63*, *Shh*, *Gli1*, *Lrg5*, *Wnt7a* and *Cd44*, but significant increases of pro-inflammatory genes, *Krt16*, *Il1b* and the apoptosis-related gene *p53*. These results suggested that Ahed expression is required for barrier function, epidermal cell survival and HF development at the embryonic stage.

Postnatal impairment in skin homeostasis of Ahed-EcKO mice

Newborn Ahed-EcKO mice (postnatal day 0, P0) appeared normal, but they showed growth retardation from P2 and all of them died before P4 (Fig. 2a). Ahed-EcKO mice at P1 harbored increased numbers of apoptotic epidermal cells (H&E staining and TUNEL immunostaining, Fig. 2b, c), which were already detectable at dpc 19.5 (Fig. 1a, b) but apparently had continued to increase. Strikingly, the expression of FLG in the granular layer had completely disappeared in P1 Ahed-EcKO mice assessed by immunostaining and western blotting (Fig. 2b, d and Supplementary Fig.S2). qRT-PCR analysis of skin tissues from Ahed-EcKO mice on P1 revealed a significant decrease in the expression of barrier function/differentiation-related genes (*Flg*, *Lor*, *Cdsn and Casp14*) and stem cell signature/HF development genes (*Ptch1*, *Gli1*, *Lgr5* and *Cd44*), but a significant upregulation of pro-inflammatory genes (*Krt16*, *Stat3*, *Il1b*, *Tnfa*, *Cxcl2*, *Cxcl1* and *S100a8*) (Fig. 2e). Western blotting and immunohistochemistry for FLG, Loricrin (LOR), Keratin (KRT)10, 14 and GLI1 reproduced the results of qRT-PCR (Fig. 2d, Supplementary Fig. S1 and S2). Further, the skin of Ahed-EcKO mice on P1 and P2 accumulated neutrophil infiltrates both in the epidermis and in the dermis, while substantially no neutrophils were found in the control (Supplementary Fig. S2 and S3a). Neutrophil migration could be attributed to the enhanced levels of chemokines in Ahed-EcKO mice (Fig. 2e). Interestingly, the number of Ki67-positive cells in HFs was significantly decreased in Ahed-EcKO mice at P1 (Supplementary Fig. S3b), suggesting there is a disturbance of HF growth (anagen) when Ahed is deficient. At P2, Ahed-EcKO mice further developed histologic abnormalities, including compact hyperorthokeratosis, loss of keratohyalin granules, epidermal hyperplasia (acanthosis), enlarged epidermal cell size, shortened HFs and inflammatory cell infiltrates in the epidermo-dermal junction and subcorneal neutrophil accumulation (Supplementary Fig. S2 and S3a). In addition, Ahed-EcKO skin at P2 showed epidermal thickening with increased number of $KRT5^+$ cells in the suprabasal layers (Supplementary Fig. S2). These findings implied that Ahed deficiency could lead to an impairment in the epidermal differentiation program and inflammatory condition. Ultrastructural analysis revealed a marked decrease of keratohyalin granules in

the epidermis of Ahed-EcKO mice (Supplementary Fig. S4), possibly due to the FLG deficiency. Correspondingly, transepidermal water loss (TEWL) was significantly increased in Ahed-EcKO mice at P2 (Fig. 2f), which strongly suggested that the impaired skin barrier function was due to the loss of barrier-associated molecules thereby leading to their early lethality. Collectively, the abnormality trends of their epidermis were inherent, but were much exaggerated after birth over time.

Epidermal alteration with inducible Ahed-KO in adult mice

To explore the role(s) of Ahed in adult skin, tamoxifen-inducible epidermis-specific Ahed deficient mice were generated by crossing Ahed $^{flox/flox}$ mice with K5.CreERT2 mice[17]. K5.CreERT2_Ahed $^{flox/flox}$ (AhedIndEcKO) mice were treated by topical application of two different doses of 4-OH tamoxifen (4OHT) on their shaved dorsal skin. No obvious macroscopic abnormalities or differences in TEWL were observed between 4OHT- and vehicle-treated skins on day 12. However, TUNEL staining revealed increased numbers of apoptotic epidermal cells in 4OHT-treated mice in a dose-dependent manner (Fig. 3a, b). Further, mice treated with a higher concentration of 4OHT exhibited focal epidermal thinning (arrowheads) and hyperkeratosis (asterisk), possibly due to cell apoptosis in the epidermis. Similar to embryonic and newborn Ahed-EcKO mice, the skin of AhedIndEcKO mice had a trend of transcriptional up-regulation of pro-inflammatory genes, including *Il1a*, *Il1b*, *Cxcl1* and *S100A8* but a down-regulation of epidermal stem cell signature genes such as *Lgr5* and *Lgr6* (Fig. 3c). However, unlike Ahed-EcKO mice, epidermal barrier/differentiation-related genes were not down-regulated in AhedIndEcKO mice (Fig. 3c). Treatment with high dose 4OHT lowered the body weight of mice from day 10 and seriously debilitated them on day 12 (Supplementary Fig. S5a, b). This might be due to dyspepsia and consequent malnutrition because of inflammatory and/or hyperkeratotic changes in the mucosal epithelia of the tongue and esophagus (Supplementary Fig. S5c), where K5 promoter-driven Ahed deletion occurred. Following treatment with a lower dose of 4OHT, however, AhedIndEcKO mice survived but exhibited eczematous lesions from day 20 to 25 (Fig. 3d). Their histologic changes included epidermal hyperplasia, hyperkeratosis and inflammatory cell infiltrates in the upper dermis (bottom panels, Fig. 3d). Together, the induced Ahed deletion in adult mice resulted in epidermal cell apoptosis and consequent eczematous changes.

Ahed disruption in vitro in primary keratinocytes

Primary epidermal keratinocytes derived from newborn Ahed-IndEcKO mice were subjected to *in vitro* treatment with 4OHT versus the vehicle control, EtOH, to analyze differential gene expression using RNA-seq (Supplementary Fig. S6). Compared with the control, 101 genes were significantly up-regulated (log2 > 1.0), whereas 135 genes were significantly down-regulated (log2 < -1.0) in Ahed KO keratinocytes. Enrichment analysis revealed that genes associated with “epithelial cell proliferation” and “keratinocyte differentiation” were among the significantly down-regulated genes. Given that the 4OHT-driven Cre-mediated deletion of *Ahed* was verified (Supplementary Fig. S7a, b), qRT-PCR analysis confirmed representative genes with differential expression (Supplementary Fig. S7c).

The 4OHT-mediated Ahed-IndEcKO keratinocytes showed a significant suppression of cell proliferation in colony forming assays during the 11 day culture relative to control groups of vehicle-treated Ahed-IndEcKO and 4OHT-treated control cells (Fig. 4a). Cell cycle assays revealed a decrease of S phase and an increase of G2/M phase in Ahed-IndEcKO keratinocytes (Fig. 4b). However, expression levels of proteins related to cell proliferation, cell cycling, apoptosis and ER stress were not altered (Fig. 4c, Supplementary Fig. S8a). Notably, Ahed-IndEcKO keratinocytes showed a reduced level of Stat3 phosphorylation (Fig. 4c, d), although there was no change in the phosphorylation status of Stat1, Jak1, Jak2 or Tyk2 (Supplementary Fig. S8a). Further, no increase was observed in the mRNA levels of phosphatases that might be involved in Stat3 dephosphorylation (Supplementary Fig. S8b). Therefore, an unknown Ahed-associated epigenetic machinery might involve Stat3 phosphorylation, which could be associated with cell proliferation.

Inter-molecular associations of Ahed with known spliceosomal proteins

Ahed was identified using Piggy-Bac transposon-based mutagenesis in murine ES cells and was found to be essential for hematopoiesis[12]. While Ahed was assumed to be a spliceosomal protein, its function(s) had largely remained elusive. Previous studies demonstrated that Ahed interacts with nuclear proteins[12,18,19]. Indeed, Ahed-GFP fusion protein-expressing HeLa cells showed nuclear localization by immunostaining (Fig. 5a). To identify Ahed binding proteins, co-immunoprecipitation and mass spectrometry analyses were performed. Proteins associated with Ahed were identified in immunoprecipitation (IP) fractions with an anti-GFP antibody by comparing GFP- and Ahed-GFP-expressing cells (Fig. 5b). In addition, the proteins that co-immunoprecipitated with Ahed were confirmed by western blotting (Fig. 5c). Although non-specific binding to NUMA1 and PSPC1 was detected, PRPF8 and SF3B1 were demonstrated to specifically associate with Ahed (Fig. 5c). Since PRPF8 and SF3B1 are known spliceosomal proteins[20], whether Ahed interacts with other spliceosomal proteins was further studied using IP-western blot assays. Anti-RBM39-immunoprecipitated proteins were found to bind to Ahed as well as PRPF8 and SF3B1 but not PRPF22 or NUMA1 (Fig. 5d), suggesting there was an association of PRPF8, SF3B1 and RBM39 with Ahed. This result strongly implied that Ahed is part of the spliceosomal protein complex. Indeed, cell immunostaining revealed that Ahed is localized in the nucleus as a speckled pattern and co-localizes with SC-35 (also known as SRSF2), a spliceosomal protein (Fig. 5e).

Cell-free assay of spliceosomal protein-protein associations with Ahed

Spliceosomes are large molecular complexes that consist of small nuclear RNAs and large numbers of proteins. Given that Ahed belongs to spliceosomes, we next studied whether there are any direct interactions between Ahed and representative spliceosomal proteins. To this end, we used a cell-free *in vitro* transcription/translation system for protein synthesis, followed by IP and western blotting, to identify proteins associated with Ahed. The results of co-immunoprecipitation assays revealed that

several spliceosomal proteins (SF3B1, PRPF22 and SLU7) were directly associated with Ahed (Fig. 6a, b). PRPF22 belongs to the DEAD box protein family, however, other DEAD box family members (PRPF16 and DHX35) were not associated with Ahed (Fig. 6b). PRPF8, a catalytic core protein of spliceosomes[21], was not co-localized with Ahed-IP in these conditions (Fig. 6a). Since the molecular weight of PRPF8 (over 200 kD) is too large to be efficiently synthesized in this system, we synthesized the smaller N- and C-terminal moieties of PRPF8 (Supplementary Fig. S8a). Western blotting revealed that there was an association of the N-terminal fragment of PRPF8 with Ahed (Fig. 6c). BRR2, an RNA helicase, mediates spliceosome catalytic activation, and its activity was found to be regulated by PRPF8[22]. Since BRR2 is also a very large molecule, we separately synthesized its N- and C-terminal moieties (Supplementary Fig. S9b). Western blotting revealed that, unlike PRPF8, the C-terminus of BRR2 bound to Ahed (Fig. 6c). SLU7, CDC40 (Prp17) and BRR2 are positioned in close proximity within spliceosomes[20,23]. Our data implied that SLU7 and BRR2 bind directly to Ahed. SF3B1 is the largest subunit of the SF3B complex, which forms a larger complex with SF3A and is involved in the U2 snRNP- the branch point sequence (BPS) recognition[24]. However, no interaction was detected between Ahed and other U2 associating proteins (SF3A1 and SF3A2 or U2AF1 and U2AF2, Supplementary Fig. S9c). Furthermore, a reverse IP experiment was performed using V5-tagged Ahed fragments to determine which of them directly interacted with spliceosomal proteins (Fig. 6d). The full length (i) and the 1-188 fragment of Ahed (ii) co-immunoprecipitated with all spliceosomal proteins examined. The 84–188 fragment (v) co-immunoprecipitated with SLU7 (Fig. 6e). Thus, the N-terminus of Ahed generally plays a critical role in the interactions with those proteins. From these findings, we propose that Ahed might be located between the known spliceosomal proteins as illustrated in Supplementary Fig. S10.

Immunostaining of the truncated Ahed-FLAG expression with an anti-FLAG antibody revealed that fragment 1–90 aa (iv) targeted both to the nucleus and the cytoplasm, although other fragments remained in the nucleus (Supplementary Fig. S11), suggesting that the NKAP domain (ND) and the basic domain (BD) are involved in the nuclear localization of Ahed.

Ahed regulates pre-RNA splicing of target genes

To determine whether Ahed is involved in RNA splicing, full-length cDNA-seq analysis was performed to identify differentially expressed RNA isoforms between wild-type and Ahed KO keratinocytes (summarized in Supplementary Fig. S12). As a result of mapping the full-length cDNA-seq read to the mouse genome (mm10), the mapping rates of control and Ahed KO cells were 92.2% and 96.2%, respectively. By gene structure prediction using StringTie, 42,813 transcripts from 18,380 loci of control and 64,883 transcripts from 21,790 loci of Ahed KO cells were predicted. After elimination of single exon genes from the predicted transcripts and comparison using GffCompare, 42.5% of the transcripts were shared between the samples, however, the rest were unique in either sample. Among the predicted transcripts, those detected in either the sample and the same gene locus were regarded as "candidates for alternative splicing isoforms". The candidate transcripts included 5,922 from the control and 21,534 from Ahed KO cells. Those unique transcripts in each sample suggested that Ahed plays distinct roles in the regulation of RNA splicing in keratinocytes.

Among the candidate genes, differentially expressed isoforms were confirmed by conventional RT-PCR analysis (Fig. 7). *Cd44* has variable isoforms when spliced at Exons 5–8, which are flanked by stable exons of the 5' and 3' termini. The largest isoform, namely CD44E, is composed of all exons and is expressed in epithelial cells including the epidermis. Strikingly, Ahed KO keratinocytes showed a marked decrease in expression of the *CD44E* isoform (714 bp) but instead, there was an increase in the smallest isoform (345 bp). *Yipf2* harbors variable Exon 8 of a different length and the larger isoform of 611 bp was increased but instead expression of the smaller isoform of 573 bp was decreased in Ahed KO keratinocytes. The shorter isoform of *Med15* (573 bp), which is due to a splice of Exon 5, was greatly decreased in KO keratinocytes. The larger isoform of *Ldb1* (405 bp) was almost absent in Ahed KO keratinocytes. Minor splicing variants with various lengths of Exon 1 of the *Cdk2* gene were altered by the Ahed deficiency. Taken together, these data clearly demonstrate that pre-RNA splicing of some genes is regulated by Ahed in keratinocytes, thereby affecting normal epidermal development and homeostasis.

Discussion

A variety of signaling pathways is required for epidermal development, homeostasis and repair, as well as for HF development and bulge stem cell maintenance. However, it was unknown whether spliceosome proteins contribute to the signaling pathways essential for epidermal homeostasis. In this study, we demonstrated that Ahed, a spliceosomal protein, plays critical roles in generating the relevant spliced mRNAs required for development and maintenance of the epidermis, which is similar to our recent finding about the involvement of Ahed in hematopoietic development[12].

Ahed-EcKO mice showed an impairment of epidermal survival and HF growth, with concomitant decreases of *p63, Shh, Gli1, Lgr5, and Cd44* gene expression, although it was not determined whether the Ahed deficiency directly caused those changes. Analyses of inducible Ahed KO mice and their keratinocytes revealed that the Ahed deficiency induced cell apoptosis as well as alterations in epidermal differentiation and pro-inflammatory changes. Indeed, RNA-seq data from inducible Ahed KO keratinocytes indicated a down-regulation of the expression of genes involved in epithelial cell proliferation and keratinocyte differentiation in accordance with results from the *in vivo* studies.

As expected from previous studies[19,25], we found that Ahed interacts with splicing-related molecules, including SF3B1, PRPF8, PRPF22, BRR2 and SLU7, *in vitro*. Recent studies have disclosed the structure of spliceosomes and related molecules that contribute to pre-RNA splicing[20,26,27]. Splicing begins with assembly of the spliceosome with target pre-RNAs. At the activation step, pre-RNAs have a loop structure, whereby the 5- and 3'-exons are arranged in close proximity. Consequently, the 5' and 3' exons are ligated and the intron lariat is dissociated at the catalysis step. PRPF8 is the largest protein in spliceosomes and is highly conserved among species and interacts with all of the chemically reactive groups of pre-mRNAs[28]. BRR2 contains two helicase cassettes and the amino-terminal cassette (NC) has helicase activity to U4/U6[29]. The BRR2 NC interacts with the PRPF8 carboxy-terminal Jab1 domain. SLU7 and PRPF22 are recruited to C* spliceosomes and bind to PRPF8. The binding of SLU7 to PRPF8 leads to

stabilization of the spliceosome. PRPF22 is thought to dissociate the ligated exon[26]. SF3B1 is a component of U2 that has a critical role in the recognition of the pre-mRNA branch point sequence and is dissociated from the spliceosome during the B^{act}-to-B^{*} transition[27]. Thus, SF3B1 does not exist simultaneously with SLU7 and PRPF22 in the spliceosomes. Our finding that Ahed interacts with PRPF22 and SLU7 but not with PRPF16 suggests that Ahed has roles in C* and/or P complex formation during the catalysis step of the pre-RNA splicing process. Recent progress in cryo-EM of spliceosomes has facilitated the structural analysis of pre-mRNA splicing in yeast and in human cells[27]. Among the interacting proteins, PRPF8, PRPF22, SLU7 and BRR2, are arranged around the specific space closely related to each other[20,23]. NKAP, which shares < 20% identical amino acids in the NKAP domain with Ahed, was reported to bind RNA and promote binding of SLU7 on PRPF8 in the C*/P complex[30,31]. Although the peptide similarity is relatively low between Ahed and NKAP, Ahed might interact with SLU7 and PRPF8, competitively with NKAP. How Ahed interacts with those spliceosomal proteins to perform mRNA splicing still remains elusive. Determination of the 3D structure of Ahed by cryo-EM analysis using an Ahed recombinant protein is needed to clarify the actual intermolecular interactions within spliceosomes.

Similar to our findings for the Ahed deficiency, knocking-down the *PRPF22* and *SLU7* genes resulted in cellular G2/M arrest[32,33], suggesting a cooperated function of PRPF8, SLU7 and Ahed within spliceosomes. In addition, disruption of the *SF3B1* gene in myeloid cell lines led to cell cycle arrest and impaired erythroid differentiation[34]. SF3B1 null mice die at the 16 to 32 cell stage[35]. PLRG1 is a component of spliceosomes and PLRG1 null mice die at embryonic day 1.5[36]. Also, *PRPF19* gene disruption suppresses cell proliferation[37]. A homozygous mutation of PRPF22 in zebrafish led to embryonic lethality with an abnormality in early hematopoietic development[38], which also occurred in Ahed deficient mice[12].

An Ahed deficiency affects STAT3 activation, which is a proliferation-related signaling molecule. This finding was in line with the notion that STAT3 signaling is critical for keratinocyte proliferation[39], although the underlying mechanism by which Ahed is involved in STAT3 phosphorylation remains elusive.

From the full-length cDNA seq data, a number of splicing variants was found in Ahed-deficient keratinocytes and some of them were confirmed by conventional PCR analysis. Among them, KO keratinocytes showed an aberrant isoform pattern of CD44, which is a transmembrane glycoprotein receptor for hyaluronic acid. It is well known that CD44 has various splicing isoforms whose expression patterns are unique in cell lineages. The standard isoform is highly expressed in many types of cells and is abundant in hematopoietic cells, whereas its longest isoform, which is composed of all the variant exons, is expressed in keratinocytes[40]. Previous studies demonstrated that epidermis-specific CD44KO mice and antisense-mediated knock-down mice were impaired in keratinocyte proliferation despite no abnormality in the skin tissue[41]. In this study, the Ahed deficiency affected CD44 isoforms through alteration of the splicing of *CD44* transcripts, however, it remained unknown whether this was the cause of the impaired keratinocyte proliferation in Ahed-KO mice. CDK2, a serine/threonine protein kinase and a

regulator of cell cycling, was found to be another target of Ahed, although its relevance to the Ahed-KO condition was undefined. Among the targets of Ahed examined, the most striking was the splicing alteration found in the *Ldb1* gene, since no spliced transcript of 405 bp derived from Exons 2 to 5 was found in Ahed-KO cells. LIM-domain binding protein 1 (LDB1) is known to be a transcriptional adaptor, playing roles in hematopoiesis, cancer development, metastasis and epithelial differentiation[42,43]. Therefore, an Ahed deficiency might affect LDB1 function required for normal epidermal homeostasis through the alteration of LDB1 isoforms, which needs further verification at the protein level.

Mutations of spliceosomal genes have been found in many diseases including various types of cancers[44–47]. Regarding the human *AHED* gene, missense mutations and truncate mutations have been identified in cancer cells in the COSMIC database (https://cancer.sanger.ac.uk/cosmic). The results of the current study revealed that Ahed has an essential role in epidermal homeostasis in an epigenetic manner, likely through the normal splicing mRNAs of genes required for cell cycling and survival. Further investigation of Ahed will pave the way to understand the importance of mRNA splicing for epigenetic regulation in the skin.

Materials and methods

Mice

Ahed flox mice were generated as described in our recent publication[12]. K5.Cre mice[48] were crossed with Ahed flox mice to generate epidermis-specific Ahed deficient mice. K5.CreERT2 mice were obtained from Jackson Lab (Bar Harbor, ME)[17] and were used to generate tamoxifen-inducible epidermis-specific Ahed deficient mice (K5.CreERT2_Ahed$^{flox/flox}$) by topical application of their shaved dorsal skin with 4-hydroxy tamoxifen (4OHT, Cayman Chemical, Ann Arbor, MI) dissolved in ethanol (EtOH) at 1.0 or 0.1 mg/ml three times, every other day. All experimental procedures performed on mice were approved by the Institutional Animal Care and Use Committee of the Kochi Medical School (I-00030, J-00071).

Measurement of TEWL

TEWL was measured using a Tewameter TM300 (Courage + Khazaka electronic GmbH, Köln, Germany) at P2.

Histological studies

Skins, other organs and whole embryos were fixed with formalin and processed for formalin-paraffin embedded sections. The sections were stained with hematoxylin and eosin (H&E). Histological images were taken using an Axio Imager A2 plus Axiocam 512 color (Zeiss, Oberkochen, Germany).

Immunostaining

Deparaffinized sections were heated at 105˚C for 10 min in 0.1 M citrate buffer (pH 6.0) using an autoclave machine for antigen retrieval, then were blocked with Dako's blocking solution (Agilent, Santa

Clara, CA) supplemented with 5% normal goat serum. The sections were then incubated overnight with primary antibodies at 4˚C, followed by washing with PBS. For fluorescence detection, the sections were incubated with Alexa488 anti-rabbit IgG (Abcam, Cambridge, UK) for 1 h, then washed with PBS and mounted with VECTASHIELD with DAPI (Vector Laboratories, Newark, CA). For chromogenic color detection, the sections were incubated with Envision + reagent (Agilent) for 1 h, followed by washing with PBS. Methyl green was used for counter staining. Images were obtained using an Axio Imager A2 plus Axiocam 512 color.

TUNEL staining

The TUNEL staining kit was obtained from Roche (Basel, Switzerland). Sections were deparaffinized and incubated at 105˚C for 10 min in 0.1 M citrate buffer, then were incubated with TUNEL reaction solution at room temperature (RT) for 1 h. After washing with PBS, sections were mounted with VECTASHIELD with DAPI and images were taken with a microscope. The number of TUNEL-positive cells in the epidermis were counted at high-magnification.

Electron microscopy

Skin samples were taken from euthanized mice at P2, and were fixed in 2.5% glutaraldehyde for 2 h, post-fixed in 1% osmium tetroxide for 2 h, dehydrated in a graded ethanol series and then embedded in epoxy resin. Semithin sections (1 μm) were stained with toluidine blue. Ultrathin sections (100 nm) were stained with uranyl acetate and lead citrate and were examined using a JEM-1400 Plus transmission electron microscope (JEOL, Tokyo, Japan).

Quantitative real-time RT-PCR analysis

Total RNAs were extracted using an RNAeasy plus kit (Qiagen, Hilden, Germany) and were reverse-transcribed using a SuperScript VILO cDNA Synthesis Kit (Thermo Fisher Scientific, Waltham, MA). Each cDNA was subjected to quantitative PCR analysis using Power SYBR Green PCR Master Mix in a StepOne™ Real-Time PCR System (Thermo Fisher Scientific). Relative mRNA expression levels were determined by normalization with hypoxanthine guanine phosphoribosyl transferase (HPRT) mRNA as a housekeeping gene. The primers used are listed in Supplementary Table S1.

Western blotting

Whole skin samples were minced and dissolved in urea solution (9 M urea, 2% Triton-100, 5% 2-mercaptoethanol). Cultured cells were lysed with RIPA buffer (Merck, Darmstadt, Germany) containing proteinase inhibitors and phosphatase inhibitors (Merck). Concentrations of proteins in samples were measured using a Protein assay kit (Bio-Rad, Hercules, CA). The lysates were separated on 4–15% gradient gels (Bio-Rad) and blotted on polyvinyl difluoride (PVDF) membranes (Bio-Rad). For blocking of the membranes, 5% skim milk or 5% bovine serum albumin in Tris buffered saline with 0.1% Tween 20 (TBST) was used. ECL Prime (Cytiva, Marlborough, MA) or SuperSignal West Atto (Thermo Fisher Scientific) were used for signal detection. X-ray films (Cytiva) were used for detection. The antibodies used in this study are listed in Supplementary Table S2.

Primary culture of murine epidermal keratinocytes

Dorsal skins of Ahed$^{flox/flox}$ and K5CreERT2_Ahed$^{flox/flox}$ newborn mice were incubated overnight with dispase (Becton Dickinson, Franklin Lakes, NJ) at 4˚C. The epidermis was then detached from the dermis and incubated with 0.25% trypsin (Thermo Fisher Scientific) for 5 min at 37˚C. After stopping the trypsin reaction with fetal bovine serum (FBS), the keratinocyte suspension was passed through a 40 μm cell strainer and inoculated in plastic apparatus. The keratinocytes were maintained in Epilife medium (Thermo Fisher Scientific) supplemented with Hu-Media KG (Kurabo, Osaka, Japan) and Y-27632 (10 μM, Cayman Chemical, Ann Arbor, MI). Keratinocytes cultured to semi-confluence were treated with 4OHT (10 nM, Cayman Chemical) for 24 h, then were cultured further for the indicated periods of time.

Colony assay

Primary murine keratinocytes were inoculated in 6-well plates at a density of 1 x 10^5 cells. The next day, the cells were treated with 4-OH tamoxifen (10 nM) for 24 h and were stained with crystal violet at day 11. The areas of keratinocytes that had grown on the dishes were measured using Image J (National Institutes of Health, Bethesda, MD).

Cell cycle analysis

Primary murine keratinocytes were treated with EtOH or 4OHT (10 nM) for 24 h. The cells were incubated with 10 μM BrdU for 2 h at day 3, and were then trypsinized and fixed with 70% EtOH for 30 min at 4˚C. The cells were incubated with 0.5% Triton-X100 in 2 N HCl for 30 min at RT and with 0.1 M sodium tetraborate, pH 8.5, for 10 min at 4˚C followed by treatment with the FITC-labeled anti-BrdU antibody (Thermo Fisher Scientific) for 30 min and with RNase solution (2 mg/mL in PBS) for 30 min after washing with 1% BSA in PBS. They were finally treated with propidium iodide (1 mg/mL) and analyzed using a LSRFortessa X-20 flow cytometer (Becton Dickinson).

Establishment of Ahed-GFP expressing HeLa cells

HeLa cells were provided by RIKEN BRC (Tsukuba, Japan) and were maintained in DMEM (Nacalai tesque, Kyoto, Japan) supplemented with 10% FBS (Thermo Fisher Scientific, Waltham, MA) and antibiotic-antimycotic solution (Thermo Fisher Scientific). The PiggyBac transposon vectors harboring green fluorescence protein (GFP) or full-length mouse Ahed-GFP and the transposase-expression vector were co-transfected to subconfluent HeLa cells using Lipofectamine 3000 (Thermo Fisher Scientific). Puromycin at a concentration of 1 μg/mL was used for selection and the surviving cell colonies were picked up using a microscope.

Identification of interacting proteins

Cell lysates were prepared from the stable transformants of GFP and Ahed-GFP expressing HeLa cells. The cells were lysed with B-300 (20 mM HEPES, 300 mM NaCl, 2 mM EDTA, 10 mM $MgCl_2$, 1% NP-40, 1 mM DTT) containing proteinase inhibitors and phosphatase inhibitors. Immunoprecipitation was

performed by incubating the lysates with anti-GFP antibody coated-magnetic beads (Medical & Biological Laboratories, Nagoya, Japan). The immunoprecipitates were dissolved and separated by SDS-PAGE followed by Coomassie Brilliant Blue staining (Integrale, Tokyo, Japan). Specific bands seen in the Ahed-GFP sample were excised and subjected to in-gel tryptic digestion. Peptides generated by the trypsin digestion were recovered and analyzed using an a LTQ XL mass spectrometer (Thermo Fisher Scientific) coupled to a Paradigm MS2 LC system (Michrom BioResouces, Auburn, CA). The MS/MS data were analyzed with an in-house database by Mascot server ver.2.3.01 (Matrix Science, Boston, MA) using Proteome Discoverer software version 1.2 (Thermo Fisher Scientific). The immunoprecipitates were also analyzed with western blotting using the indicated antibodies. For immunoprecipitation with the anti-RBM39 antibody, the antibody was pre-incubated with Protein G mag Sepharose (Cytiva) for 1 h at RT, after which the antibody-Sepharose complex was incubated with the Ahed-GFP expressing HeLa cell lysate for 2 h at 4˚C followed by 3 washes with B-300 buffer. The samples were incubated with 1x SDS sample buffer and subjected to western blot analysis.

In vitro binding assay

Full length or fragments of cDNA were prepared by RT-PCR, for which normal human keratinocyte cDNA served as a template using KOD Plus Neo (Toyobo, Osaka, Japan). FLAG and V5 epitope coding sequences were added to the 3’ end of Ahed and candidate proteins at the 3’ end of their cDNAs, respectively. cDNA fragments were introduced into the pcDNA6.2 vector (Thermo Fisher Scientific) using an infusion cloning system (Takara, Kusatsu, Japan). The sequences were confirmed by Sanger sequencing using a 3130 Genetic Analyzer (Thermo Fisher Scientific). Ahed and other candidate protein expressing vectors were added into the TnT Quick Coupled Transcription/Translation System (Promega, Madison, WI) and incubated for 90 min at 30˚C. The reaction mixture (50 µL) was mixed with 150 µL TBST with a proteinase and phosphatase inhibitor cocktail. The diluted reaction mixtures were incubated with Mag beads conjugated to anti-FLAG or V5 antibodies (Medical & Biological Laboratories) for 2 h at 4˚C. The Mag beads were washed with TBST and incubated with 1x SDS PAGE sample buffer (Fujifilm Wako, Osaka, Japan). The samples were then analyzed by immunoprecipitation followed by western blotting.

Immunofluorescence cell staining

Ahed-GFP expressing HeLa cells were inoculated in type I collagen (Nippi, Tokyo, Japan) coated 4-well chamber slides (Thermo Fisher Scientific). The cells were fixed with 4% paraformaldehyde in phosphate buffer for 30 min at 4˚C and then blocked with Dako’s blocking solution (Agilent) supplemented with 5% normal goat serum for 1 h at RT. The cells were incubated with a rabbit anti-GFP antibody (Cell Signaling, Danvers, MA) and a mouse anti-SC-35 antibody (Abcam) overnight at 4˚C. After washing with PBS, the cells were incubated with AlexaFluor488 anti-rabbit IgG and AlexaFluor594 anti-mouse IgG (Abcam) for 1 h at RT, washed with PBS, and mounted with DAPI containing VECTASHIELD. Images were taken using an Axio Imager A2 plus Axiocam 512 color (Zeiss).

Identification of domains that are essential for nuclear localization

HeLa cells were inoculated in type I collagen (Nippi) coated 4-well chamber slides (Thermo Fisher Scientific) 1 day before transfection. The Ahed-FLAG expression vectors used in the in vitro binding assay were transfected into the cells with Lipofectamine 3000 (Thermo Fisher Scientific). The cells were fixed with 4% paraformaldehyde in phosphate buffer for 30 min at 4˚C at 48 h after transfection and were blocked with Dako's blocking solution supplemented with 5% normal goat serum for 1 h at RT. The cells were then incubated with the anti-FLAG antibody (Medical & Biological Laboratories) overnight at 4˚C. After washing with PBS, the cells were incubated with Alexa488 anti-rabbit IgG (Abcam) for 1 h at RT, washed with PBS and then mounted with DAPI containing Vectashield.

mRNA-seq analysis

Total RNAs were prepared using a RNeasy kit (Qiagen) following the manufacturer's instructions. RNA quality was assessed using a Bioanalyzer (Agilent). The libraries were prepared using Illumina TruSeq Stranded mRNA Sample Preparation Kits (Illumina, San Diego, CA, USA). The poly-A containing mRNAs were purified from 0.5 μg of each total RNA using poly-T oligo-attached magnetic beads. Following purification, each mRNA was fragmented into small pieces using divalent cations under an elevated temperature. The cleaved RNA fragments were copied into first strand cDNAs using reverse transcriptase and random primers, followed by second strand cDNA synthesis using DNA Polymerase I and RNase H. These cDNA fragments then underwent the addition of a single 'A' base and subsequent ligation of the adapter. The products were then purified and enriched with PCR to create the final cDNA library with inserts ranging in size from 120–200 bp. The quality of each library was evaluated using a 2100 Bioanalyzer (Agilent) followed by paired-end sequencing on an Illumina HiSeq 2000. The sequencing run and the base call analysis were performed according to the HiSeq 2000 System Guide with TruSeq SBS kit v3-HS. After the sequencing, sequence raw data were generated by processing with cBot v3.0. RNA-seq reads were mapped to the mm10 reference genome with STAR. Exon-level read counts and differential exon usage were calculated based on exons defined in Ensembl gene annotation (Mus_musculus.GRCm38.97.chr.gtf, retrieved from http://ftp.ensembl.org/pub/release-97/gtf/mus_musculus/) using DEXseq. Enrichment analysis of differentially expressed genes was performed with Metascape (https://metascape.org[49]).

Cap Trap RNA (CTR)-seq analysis for full-length cDNA sequencing

cDNAs were synthesized from 5 μg total RNA using a RT primer (5-GAGATGTCTCGTGGGCTCGGTTTTTTTTTTTTTTTVN-3) and PrimeScript II Reverse Transcriptase (Takara Bio, Kusatsu, Japan). The full-length cDNA selection and the 5' adapter ligation were carried out using the Cap Trapper method[50]. The 5' adapter ligated full-length cDNA was amplified using Prime STAR CXL DNA Polymerase (Takara Bio) and PCR primers (5- GTGGTATCAACGCAGAGTAC-3 and 5-

GAGATGTCTCGTGGGCTCGG-3). After 15 cycles of PCR (10 min elongation time), PCR amplified full-length cDNAs were subjected to Nanopore sequencing libraries preparation using FLO-MIN10 (R10 Version) and SQK-LSK109 kit (Oxford Nanopore Technologies, Oxford, UK). Nanopore sequencing was performed on MinION MK1b device with MinION Flow Cell R10.0. The MinKNOW software version was 1.5.12. Base calling was performed using guppy_basecaller_v3_4_5 with the Basecall Barcoding workflow. Data processing of MinION sequence reads was carried out using three pieces of software as follows; Quality Check of the sequence reads using pycoQC version 2.5.0.3, Genome Mapping of the reads to the reference mouse genome mm10 using minimap2 version 2.12-r827 and Adapter Trimming using porechop version 0.2.3, respectively. Raw reads of the full-length cDNA-seq were mapped to the mm10 reference genome using Minimap2 version 2.12-r827. Exon-intron structures were inferred based on the mapping results, and transcript sequences were reconstructed by StringTie v2.1.4 with reference to the mouse gene annotation (Mus_musculus.GRCm38.101.chr.gff3, retrieved from ftp://ftp.ensembl.org/pub/release-101/gff3/mus_musculus/). After the removal of single-exon transcripts, the remaining transcripts were compared between the control and knockout samples using GffCompare v0.12.1 to detect transcripts unique to each sample. Among them, transcripts derived from the same locus were defined as candidates for alternative splicing isoforms.

Statistical analysis

SPSS (ver. 24, IBM, Armonk, NY) was used for statistical analysis. For comparison of two groups, the analysis was performed by Student’s t-test or Welch's t-test. One way ANOVA followed by the Tukey HSD test was used to compare more than three groups. $P < 0.05$ is considered significant.

Declarations

Acknowledgments

This research was supported by JSPS KAKENHI Grant Numbers JP19K08773 (M.T.), JP17K16343 (T.I.), and by the Platform Project for Supporting Drug Discovery and Life Science Research (Basis for Supporting Innovative Drug Discovery and Life Science Research (BINDS)) from AMED under Grant Number JP19am0101102 (support number 1439). We thank Misses Reiko Kamijima, Tomoko Nagayama and Chisa Matsuoka for technical assistance.

Author contributions

M.T. and T.I. designed the experiments, performed most of the experiments, analyzed the data and wrote the manuscript. K.Y. performed electron microscopy. S.K. performed flow cytometry. M.K. performed Sanger sequencing. K.M. performed mass-spectrometry. S.N., C.T. and Y.O. performed RNA-seq and full-length cDNA-seq analyses. S.K. and K.I. performed bioinformatic analysis. M.T., C.K. and J.T. provided critical materials and advice on data interpretation. S.S. supervised this project, designed the experiments and wrote the manuscript.

References

1. Singh, J. Harnessing the power of genetics: fast forward genetics in Caenorhabditis elegans. Mol Genet Genomics 296, (2021).
2. Boulin, T. & Bessereau, J. L. Mos1-mediated insertional mutagenesis in Caenorhabditis elegans. Nat Protoc 2, 1276–1287 (2007).
3. Jorgensen, E. M. & Mango, S. E. The art and design of genetic screens: caenorhabditis elegans. Nat Rev Genet 3, 356–369 (2002).
4. Venken, K. J. T. & Bellen, H. J. Chemical mutagens, transposons, and transgenes to interrogate gene function in Drosophila melanogaster. Methods 68, 15–28 (2014).
5. St Johnston, D. The art and design of genetic screens: Drosophila melanogaster. Nat Rev Genet 3, 176–188 (2002).
6. Kettleborough, R. N. W. *et al.* A systematic genome-wide analysis of zebrafish protein-coding gene function. Nature 496, 494–497 (2013).
7. Lawson, N. D. & Wolfe, S. A. Forward and reverse genetic approaches for the analysis of vertebrate development in the zebrafish. Dev Cell 21, 48–64 (2011).
8. Stanford, W. L., Cohn, J. B. & Cordes, S. P. Gene-trap mutagenesis: past, present and beyond. Nat Rev Genet 2, 756–768 (2001).
9. Kile, B. T. & Hilton, D. J. The art and design of genetic screens: mouse. Nat Rev Genet 6, 557–567 (2005).
10. Mohr, S. E. & Perrimon, N. RNAi screening: new approaches, understandings, and organisms. Wiley Interdiscip Rev RNA 3, 145–158 (2012).
11. Horie, K. *et al.* A homozygous mutant embryonic stem cell bank applicable for phenotype-driven genetic screening. Nat Methods 8, 1071–1081 (2011).
12. Nakai, R. *et al.* A new gene Ahed plays essential roles in hematopoiesis through RNA splicing. *in submission* (2023).
13. Fuchs, E. & Blau, H. M. Tissue stem cells: Architects of their niches. Cell Stem Cell 27, 532–556 (2020).
14. Li, K. N. & Tumbar, T. Hair follicle stem cells as a skin-organizing signaling center during adult homeostasis. EMBO J 40, e107135 (2021).
15. Byrne, C., Tainsky, M. & Fuchs, E. Programming gene expression in developing epidermis. Development 120, 2369–2383 (1994).
16. Mokry, J. & Pisal, R. Development and Maintenance of Epidermal Stem Cells in Skin Adnexa. Int J Mol Sci 21, 1–14 (2020).
17. van Keymeulen, A. *et al.* Distinct stem cells contribute to mammary gland development and maintenance. Nature 479, 189–193 (2011).

18. Oughtred, R. *et al.* The BioGRID database: A comprehensive biomedical resource of curated protein, genetic, and chemical interactions. Protein Sci 30, 187–200 (2021).
19. Huttlin, E. L. *et al.* Dual proteome-scale networks reveal cell-specific remodeling of the human interactome. Cell 184, 3022–3040.e28 (2021).
20. Kastner, B., Will, C. L., Stark, H. & Lührmann, R. Structural Insights into Nuclear pre-mRNA Splicing in Higher Eukaryotes. Cold Spring Harb Perspect Biol 11, (2019).
21. Grainger, R. J. & Beggs, J. D. Prp8 protein: at the heart of the spliceosome. RNA 11, 533–557 (2005).
22. Mozaffari-Jovin, S. *et al.* Novel regulatory principles of the spliceosomal Brr2 RNA helicase and links to retinal disease in humans. RNA Biol 11, 298–312 (2014).
23. Zhan, X., Yan, C., Zhang, X., Lei, J. & Shi, Y. Structure of a human catalytic step I spliceosome. Science 359, 537–545 (2018).
24. Gozani, O. R., Potashkin, J. & Reed, R. A Potential Role for U2AF-SAP 155 Interactions in Recruiting U2 snRNP to the Branch Site. Mol Cell Biol 18, 4752–4760 (1998).
25. Oughtred, R. *et al.* The BioGRID database: A comprehensive biomedical resource of curated protein, genetic, and chemical interactions. Protein Sci 30, 187–200 (2021).
26. Yan, C., Wan, R. & Shi, Y. Molecular Mechanisms of pre-mRNA Splicing through Structural Biology of the Spliceosome. Cold Spring Harb Perspect Biol 11, (2019).
27. Wan, R., Bai, R., Zhan, X. & Shi, Y. How Is Precursor Messenger RNA Spliced by the Spliceosome? Annu Rev Biochem 89, 333–358 (2020).
28. Grainger, R. J. & Beggs, J. D. Prp8 protein: at the heart of the spliceosome. RNA 11, 533–557 (2005).
29. Santos, K. F. *et al.* Structural basis for functional cooperation between tandem helicase cassettes in Brr2-mediated remodeling of the spliceosome. Proc Natl Acad Sci U S A 109, 17418–17423 (2012).
30. Burgute, B. D. *et al.* NKAP is a novel RS-related protein that interacts with RNA and RNA binding proteins. Nucleic Acids Res 42, 3177–3193 (2014).
31. Fica, S. M., Oubridge, C., Wilkinson, M. E., Newman, A. J. & Nagai, K. A human postcatalytic spliceosome structure reveals essential roles of metazoan factors for exon ligation. Science 363, 710–714 (2019).
32. Zanini, I. M. Y., Soneson, C., Lorenzi, L. E. & Azzalin, C. M. Human cactin interacts with DHX8 and SRRM2 to assure efficient pre-mRNA splicing and sister chromatid cohesion. J Cell Sci 130, 767–778 (2017).
33. Jiménez, M. *et al.* Splicing events in the control of genome integrity: role of SLU7 and truncated SRSF3 proteins. Nucleic Acids Res 47, 3450–3466 (2019).
34. Dolatshad, H. *et al.* Disruption of SF3B1 results in deregulated expression and splicing of key genes and pathways in myelodysplastic syndrome hematopoietic stem and progenitor cells. Leukemia 29, 1092–1103 (2015).
35. Isono, K., Mizutani-Koseki, Y., Komori, T., Schmidt-Zachmann, M. S. & Koseki, H. Mammalian polycomb-mediated repression of Hox genes requires the essential spliceosomal protein Sf3b1.

Genes Dev 19, 536–541 (2005).
36. Kleinridders, A. *et al.* PLRG1 is an essential regulator of cell proliferation and apoptosis during vertebrate development and tissue homeostasis. Mol Cell Biol 29, 3173–3185 (2009).
37. Yano, K. *et al.* PRPF19 regulates p53-dependent cellular senescence by modulating alternative splicing of MDM4 mRNA. J Biol Chem 297, 100882 (2021).
38. English, M. A. *et al.* Incomplete splicing, cell division defects, and hematopoietic blockage in dhx8 mutant zebrafish. Dev Dyn 241, 879–889 (2012).
39. Miyoshi, K. *et al.* Stat3 as a therapeutic target for the treatment of psoriasis: a clinical feasibility study with STA-21, a Stat3 inhibitor. J Invest Dermatol 131, 108–117 (2011).
40. Ponta, H., Sherman, L. & Herrlich, P. A. CD44: from adhesion molecules to signalling regulators. Nat Rev Mol Cell Biol 4, 33–45 (2003).
41. Shatirishvili, M. *et al.* Epidermal-specific deletion of CD44 reveals a function in keratinocytes in response to mechanical stress. Cell Death Dis 7, (2016).
42. Liu, G. & Dean, A. Enhancer long-range contacts: The multi-adaptor protein LDB1 is the tie that binds. Biochim Biophys Acta Gene Regul Mech 1862, 625–633 (2019).
43. Sugihara, T. M., Bach, I., Kioussi, C., Rosenfeld, M. G. & Andersen, B. Mouse deformed epidermal autoregulatory factor 1 recruits a LIM domain factor, LMO-4, and CLIM coregulators. Proc Natl Acad Sci U S A 95, 15418–15423 (1998).
44. Anczukow, O. & Krainer, A. R. Splicing-factor alterations in cancers. RNA 22, 1285–1301 (2016).
45. Urbanski, L. M., Leclair, N. & Anczuków, O. Alternative-splicing defects in cancer: Splicing regulators and their downstream targets, guiding the way to novel cancer therapeutics. Wiley Interdiscip Rev RNA 9, (2018).
46. Griffin, C. & Saint-Jeannet, J. P. Spliceosomopathies: Diseases and mechanisms. Dev Dyn 249, 1038–1046 (2020).
47. Yang, H., Beutler, B. & Zhang, D. Emerging roles of spliceosome in cancer and immunity. Protein Cell 13, 559–579 (2022).
48. Tarutani, M. *et al.* Tissue-specific knockout of the mouse Pig-a gene reveals important roles for GPI-anchored proteins in skin development. Proc Natl Acad Sci U S A 94, 7400–7405 (1997).
49. Zhou, Y. *et al.* Metascape provides a biologist-oriented resource for the analysis of systems-level datasets. Nat Commun 10, 1523 (2019).
50. Morioka, M. S. *et al.* Cap Analysis of Gene Expression (CAGE): A Quantitative and Genome-Wide Assay of Transcription Start Sites. Methods Mol Biol 2120, 277–301 (2020).

Figures

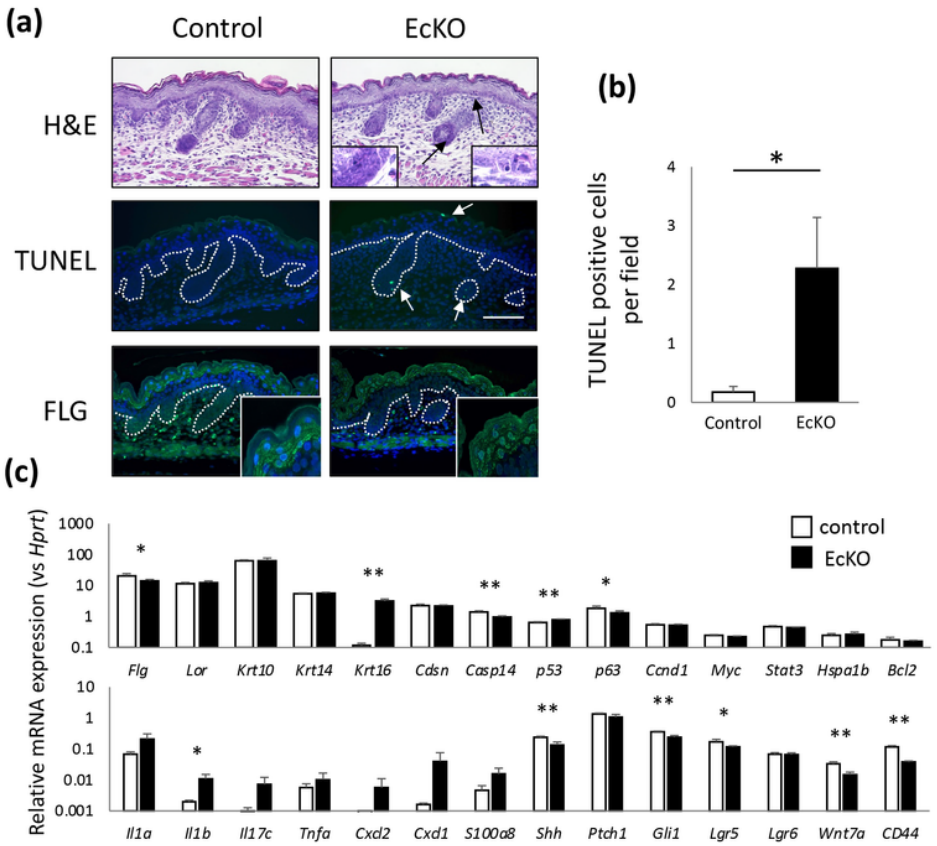

Figure 1

Figure 1

Skin abnormalities of epidermal-specific Ahed KO (EcKO) mice at 19.5 dpc. a Increased number of apoptotic keratinocytes in the epidermis and in hair follicles of EcKO mice. Cells with an eosinophilic cytoplasm and pyknotic nuclei in EcKO embryos (black arrows and insets in top panels), H&E staining. TUNEL staining (white arrows in middle panels). Immunofluorescence for filaggrin (FLG) (bottom panels, higher magnified images in insets). White dotted lines, epidermal-dermal boundary; Bar, 100 μm. **b** Number of TUNEL-positive cells (means ± s.d.) in 10 randomly selected non-overlapping fields at high magnification. n = 4; *, $p < 0.05$ by Welch's t-test. **c** Relative mRNA expression levels (means ± s.d.) determined by qRT-PCR analysis in the skin of control mice (white bars) and EcKO mice (black bars). n = 4; *, $p < 0.05$; **, $p < 0.01$ by Welch's t-test.

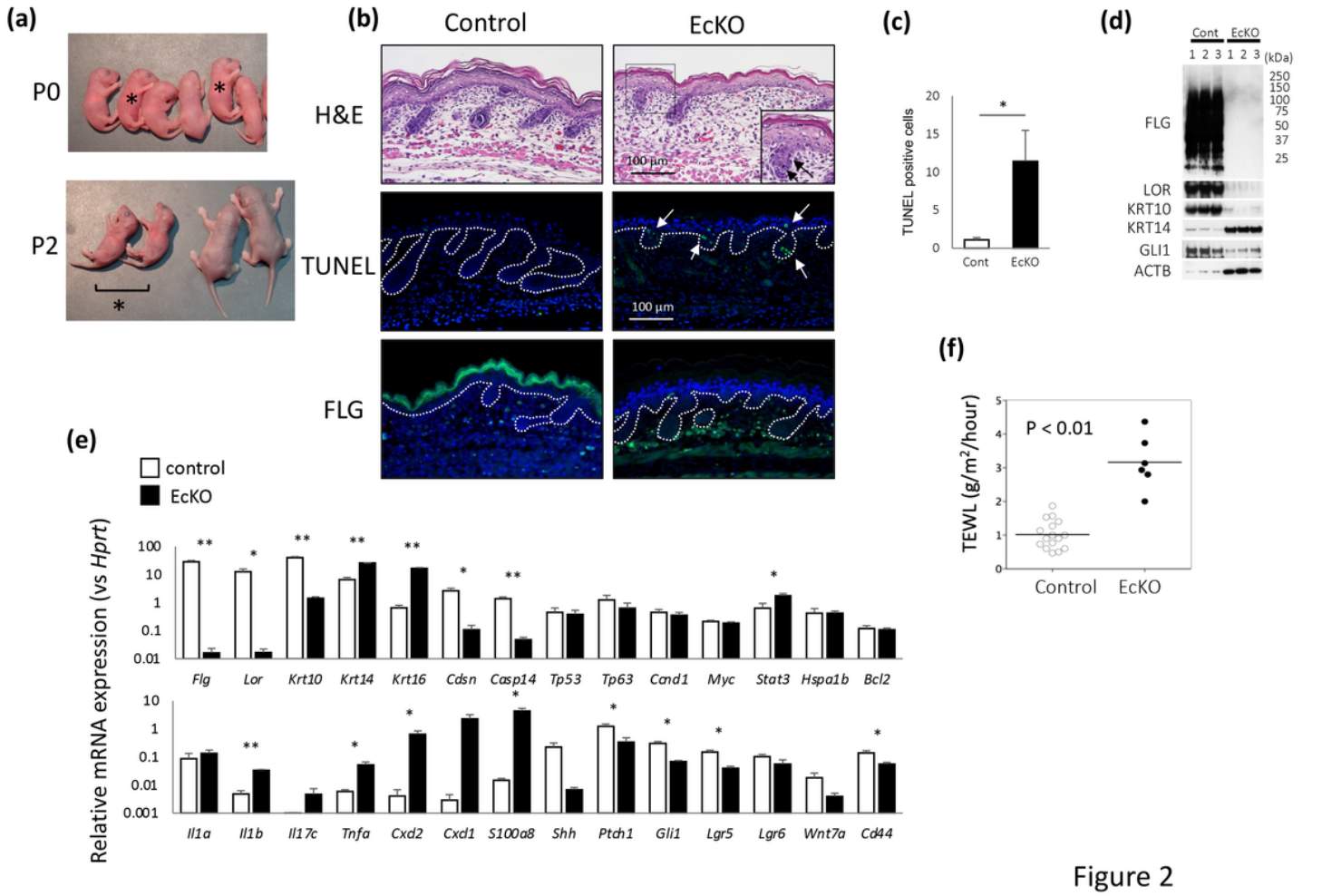

Figure 2

Figure 2

Abnormal skin in newborn Ahed EcKO mice. a EcKO mice (*) and control littermates at postnatal day 0 (P0) and P2. **b**Histological manifestations at P1. Apoptotic cells indicated by H&E staining (arrows, upper panels), TUNEL staining (white arrows, middle panels). Immunostaining for filaggrin (FLG) (lower panels). White dotted lines, epidermal-dermal boundary; bar, 100 µm. **c** Number of TUNEL-positive cells (means ± s.d.) in 10 randomly selected non-overlapping fields at high magnification. n = 4; *, $p < 0.05$ by Welch's t-test. **d** Western blotting of whole skins excised from euthanized mice at P1. LOR, loricrin; KRT, keratin; ACB, b-actin. **e** Relative mRNA expression levels (means ± s.d.) determined by qRT-PCR analysis in whole skin of control mice (white bars) and EcKO mice (black bars). n = 3; *, $p < 0.05$; **, $p < 0.01$ by Welch's t-test. **f** Trans-epidermal water loss at P2. Welch's t-test.

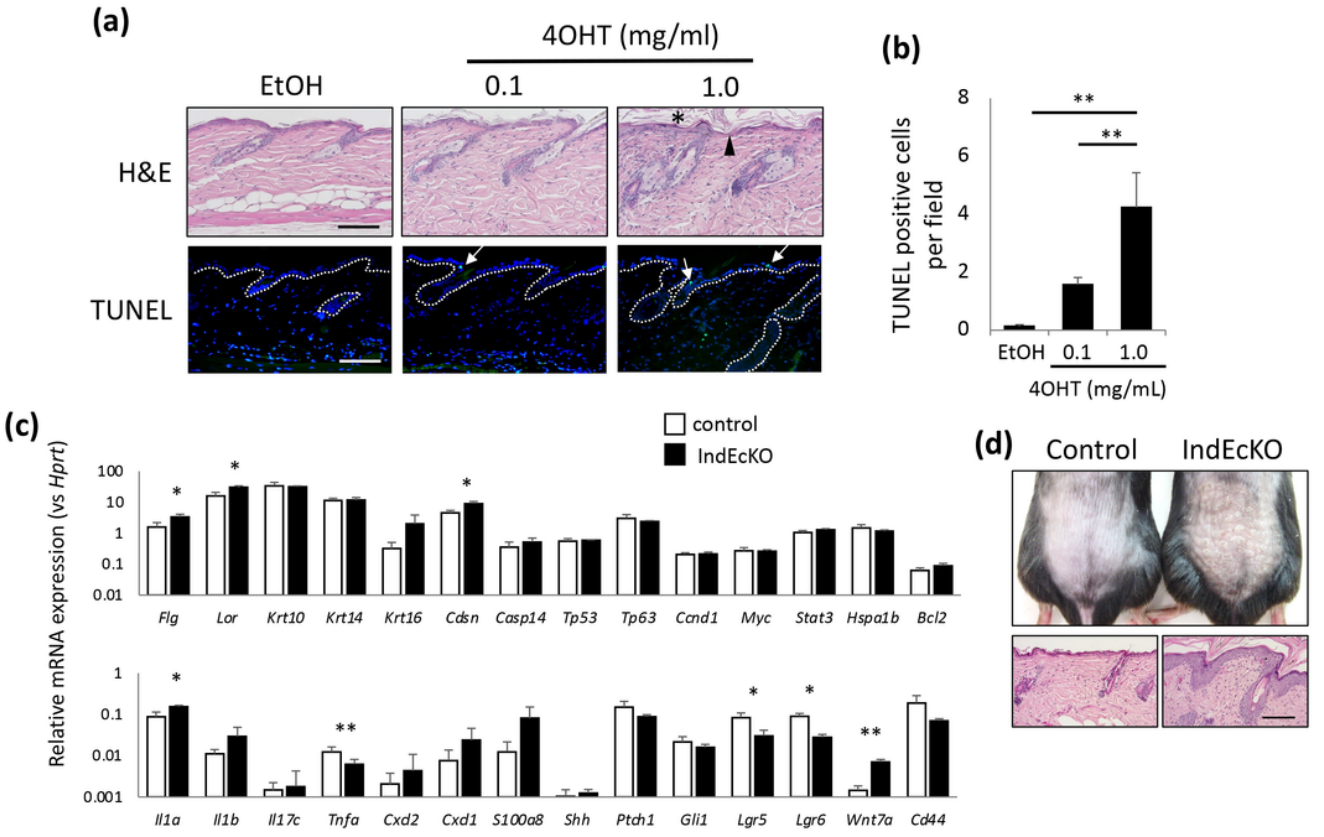

Figure 3

Figure 3

An Ahed deficiency in adult mouse skin results in epidermal cell death. a Histological (H&E staining, top panels) and TUNEL staining (bottom panels) of skins from K5.CreERT2_Ahed KO (IndEcKO) mice topically treated with ethanol (EtOH) or 4-OH Tamoxifen (4OHT at concentrations of 0.1 or 1.0 mg/mL) on days 1, 3 and 5, then sampled at day 12. *, parakeratosis; arrowhead, focal epidermal atrophy; white arrows, TUNEL-positive cells; white dotted lines, epidermal-dermal boundary; bars, 100 µm. **b** Number of TUNEL-positive cells in the IFE and in HFs. n = 3. **; p <0.01 by Tukey HSD. **c** Relative mRNA expression levels (means ± s.d.) of the indicated genes using qRT-PCR analysis in whole skin of control mice (white bars) and IndEcKO mice (black bars) treated with 1.0 mg/ml 4OHT. n = 3; *, $p < 0.05$; **, $p < 0.01$ by Welch's t-test. **d**Macroscopic and histologic views (H&E staining) of skins from mice on day 25 after treatment with 4OHT at 0.1 mg/ml. Bar, 100 µm.

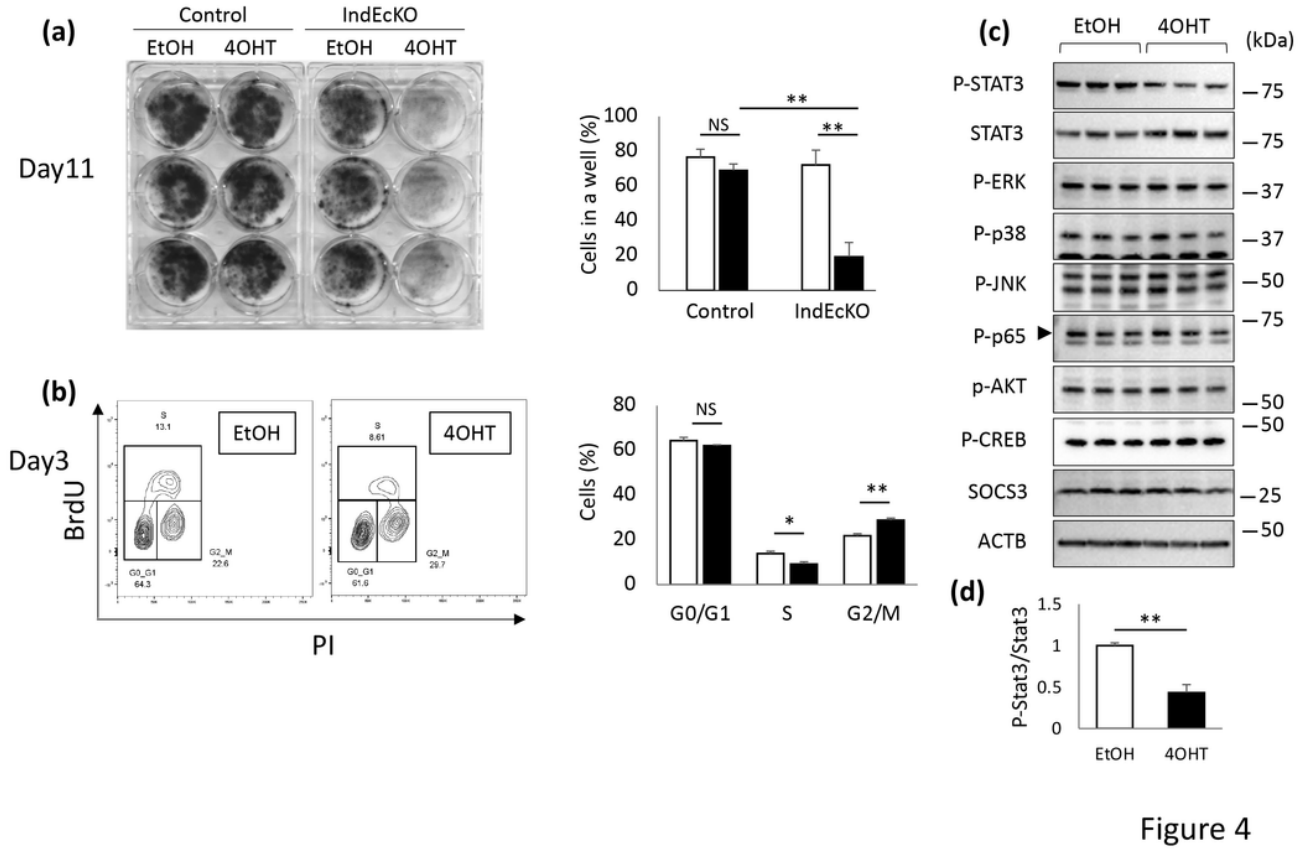

Figure 4

Figure 4

Impaired proliferation of Ahed KO keratinocytes. a Left, Epidermal cells from IndEcKO mice and from control mice *in vitro*treated with 4OHT (10 nM) or EtOH for 24 h, then stained with crystal violet at day 11. Right, Percent cells shown are the ratio of crystal violet-stained areas relative to the whole area of the culture well. Control and IndEcKO cells treated with 4OHT (black bars) or EtOH (white bars). n = 3; NS, not significant; **, p<0.01 by one way ANOVA, Tukey HSD test. **b** Cell cycle analysis using BrdU/propidium iodide (PI) incorporation in IndEcKO cells assessed by flow cytometry at day 3 of 4OHT treatment (black bars). Percent cells in each well after treatment with 4OHT compared with EtOH-treated control (white bars). n = 3, NS, not significant; *, p<0.05; **, p<0.01 by Student's t-test. **c** Western blotting of proliferation-related proteins using 4OHT-treated versus EtOH-treated IndEcKO cells. Arrowhead indicates phosphorylated NFκb p65 (P-p65). **d** Densitometric ratio of western blot bands for P-Stat3 relative to total Stat3 after normalization with b-actin. n = 3, **, p<0.01 by Student's t-test.

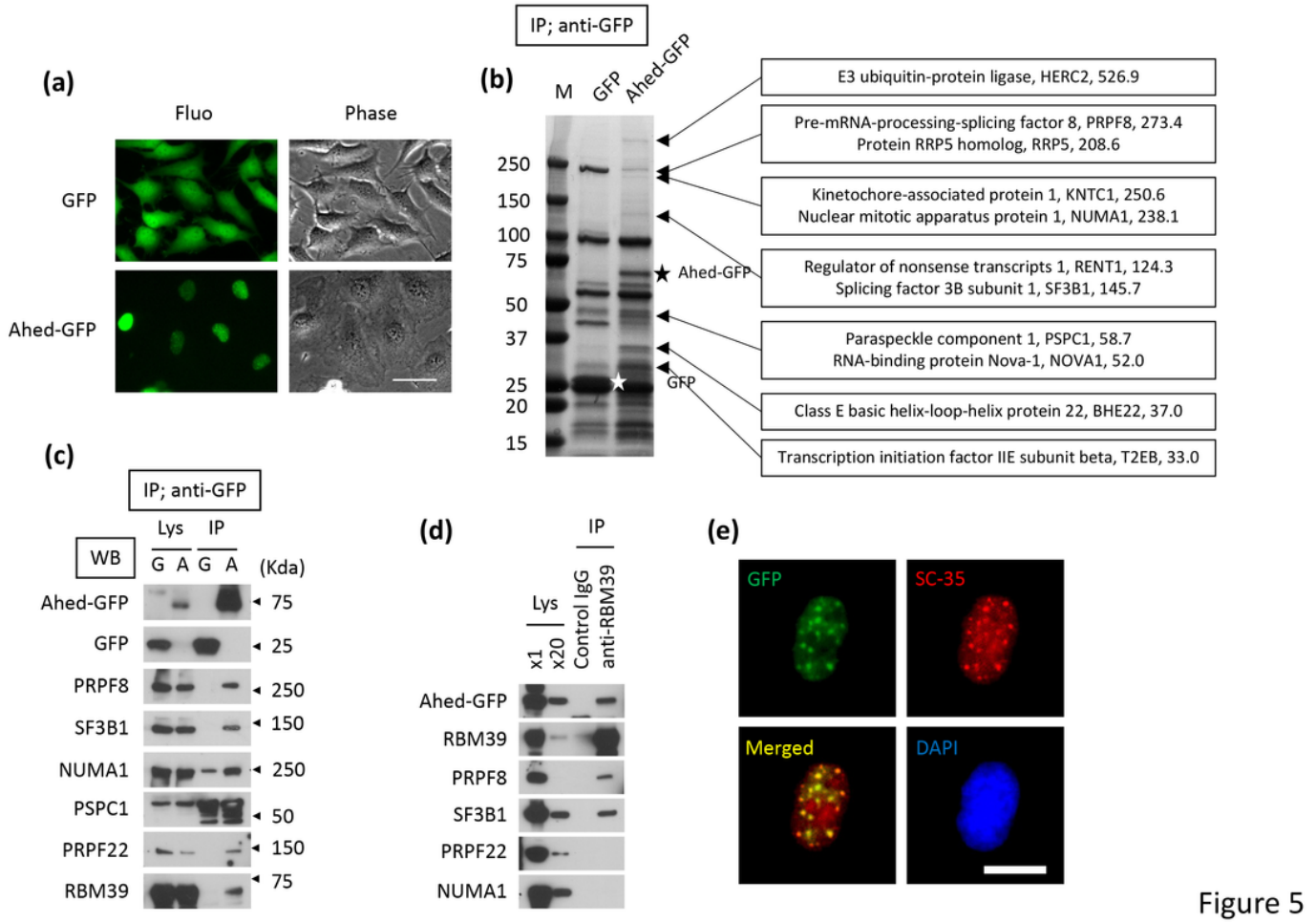

Figure 5

Figure 5

Identification of Ahed binding proteins. a Fluorescence (Fluo) and phase contrast images (Phase) of HeLa cells expressing GFP or Ahed-GFP fusion protein. Bar, 50 μm. **b** Immunoprecipitation with the anti-GFP antibody followed by Coomassie Brilliant Blue staining. Arrows indicate molecules identified by mass spectrometry. White star, GFP; black star, Ahed-GFP; M, molecular marker. **c** Western blotting of the indicated proteins in whole cell lysates (Lys) and immunoprecipitates (IP) from GFP (G) and GFP-Ahed (A) expressing HeLa cells. **d** Immunoprecipitation of GFP-Ahed expressing HeLa cell lysates with an anti-RBM39 antibody or a control rabbit IgG followed by western blotting for the indicated proteins. **e** Immunostaining of GFP-Ahed expressing HeLa cells with anti-GFP and anti-SC-35 antibodies. DAPI indicates nuclear staining. Bar, 10 μm.

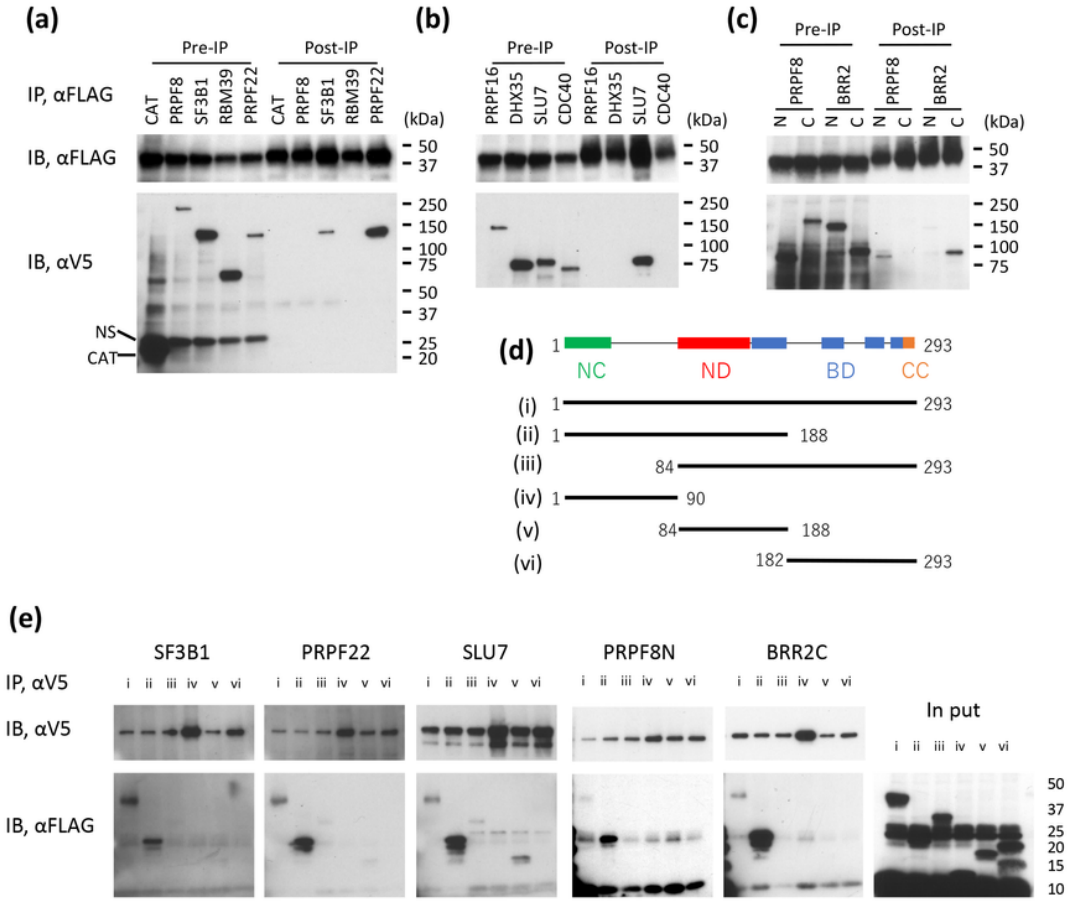

Figure 6

Figure 6

Direct interaction of spliceosomal proteins with Ahed in a cell-free system.

a - **c** Ahed and candidate proteins tagged with FLAG and V5, respectively, were synthesized using an *in vitro* transcription/translation system. IP, immunoprecipitation; IB, immunoblotting; NS, nonspecific; CAT, chloramphenicol acetyltransferase. **d** Schematic of synthesized full length (i) and truncated (ii to vi) Ahed protein; numbers of amino acids are shown. NC, N-terminal conserved region; ND, NKAP domain; BD, basic amino acid rich domain; CC, C-terminal conserved region. **e** Immunoblotting of FLAG-tagged full length and truncated Ahed (i to vi) in anti-V5 immunoprecipitated proteins as indicated.

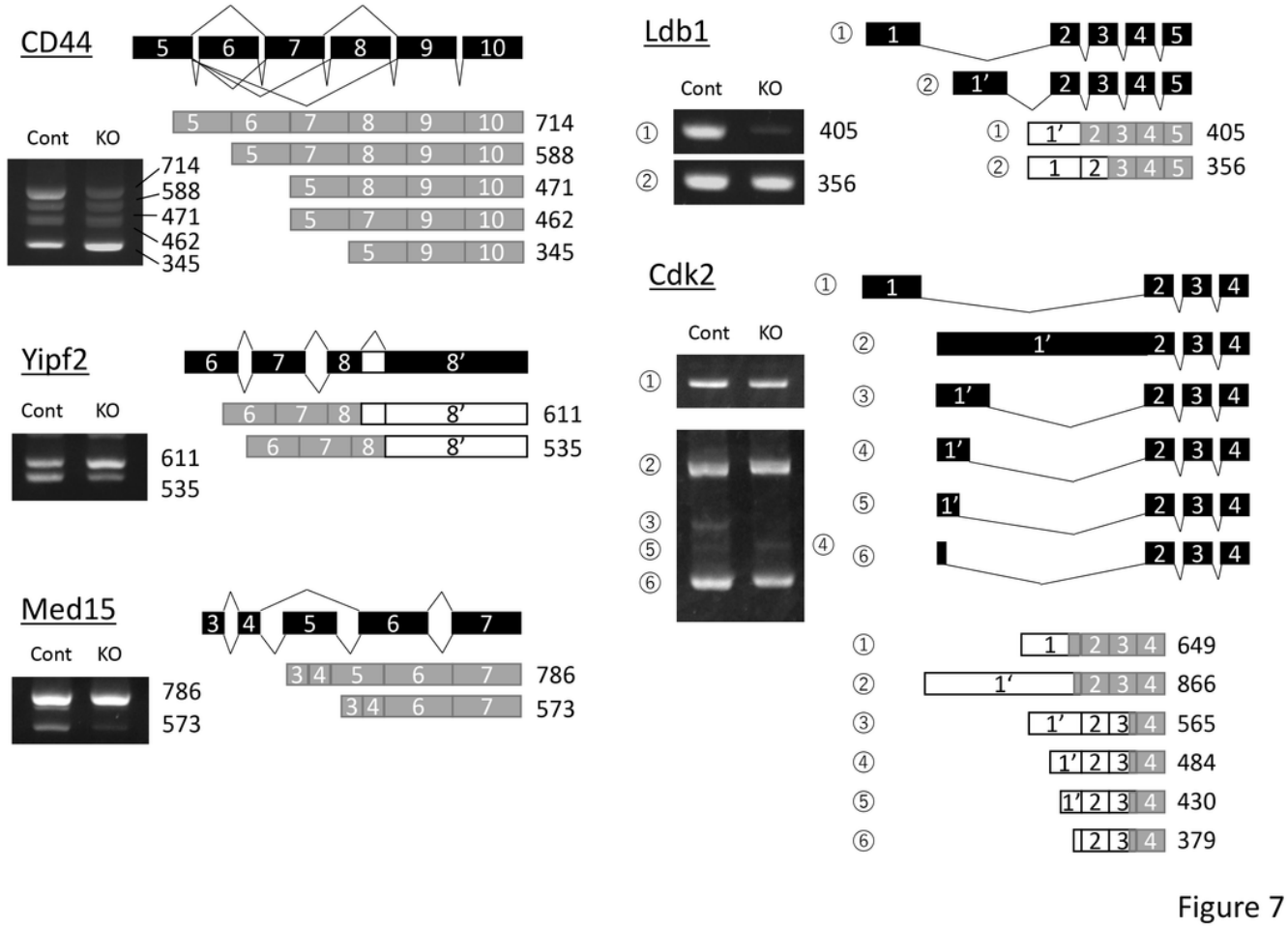

Figure 7

Figure 7

Ahed KO affects the splicing of some genes. cDNAs from epidermal keratinocytes derived from IndEcKO mice (KO) and from control mice (Cont) were used for PCR analysis to detect splicing variants. Target exons are presented as black boxes. Splicing variants amplified with specific primer sets are shown as gray (coding sequence) and white boxes (non-coding sequence). Shown are sizes of transcripts from corresponding amplicons.

Supplementary Files

This is a list of supplementary files associated with this preprint. Click to download.

- Suppl.TableS1.xlsx
- Suppl.TableS2.xlsx
- finalSupplFigs.pdf
- finalSupplementarydata.docx